Supplementary information

Table S1 – Overview of mutagenesis of residues involved in GABA recognition in $GABA_{A/C}$ receptors and conservation in ELIC

		$GABA_AR$	$GABA_CR$	ELIC
loop A	β2 (+)	Y97 [a,b] L99 [a]	D136 [j] F138 [j] V140 [j]	A75 E77 I79
loop B	β2 (+)	Y159 [b,c] Y161 [c]	Y198 [k,l] Y200 [k]	F133 Y135
loop C	β2 (+)	T202 [b] S204 [c] Y205 [a,c] R207 [c] S209 [c]	Y241 [k] T243 [k] Y247 [k,l] R249 [m]	S179 E187 F188 R190 T192
loop D	α1 (-)	F64 [d] R66 [d] S68 [d]	Y102 [k] R104 [k,m]	Y38 V40 Q42
loop E	α1 (-)	R120 [g] I121 [f]	V155 [k] M156 [k] R158 [m] V159 [k] S168 [k,m] R170 [k,m]	K90 R91 M93 L95 N104 R106
loop F	α1 (-)	V178 [h] V180 [h] D183 [h]		T150 N152 N155

[a] Unnatural amino acid mutagenesis of the GABA(A) receptor binding site residues reveals a novel cation-pi interaction between GABA and beta2Tyr97. Padgett CL, Hanek AP, Lester HA, Dougherty DA, Lummis SC. J Neurosci. (2007) 27(4):886-92.

[b] GABAA receptor needs two homologous domains of the beta-subunit for activation by GABA but not by pentobarbital. Amin J, Weiss DS. Nature. (1993) 366(6455):565-9.

[c] Structure and dynamics of the GABA binding pocket: A narrowing cleft that constricts during activation. Wagner DA, Czajkowski C. J Neurosci. (2001) 21(1):67-74.

[d] Mapping the agonist binding site of the GABAA receptor: evidence for a beta-strand. Boileau AJ, Evers AR, Davis AF, Czajkowski C. J Neurosci. (1999) 19(12):4847-54.

[e] Tyrosine 62 of the gamma-aminobutyric acid type A receptor beta 2 subunit is an important determinant of high affinity agonist binding. Newell JG, Davies M, Bateson AN, Dunn SM. J Biol Chem. (2000) 275(19):14198-204.

[f] Decreased agonist sensitivity of human GABA(A) receptors by an amino acid variant, isoleucine to valine, in the alpha1 subunit. Westh-Hansen SE, Rasmussen PB, Hastrup S, Nabekura J, Noguchi K, Akaike N, Witt MR, Nielsen M. Eur J Pharmacol. (1997) 329(2-3):253-7.

[g] Arginine residue 120 of the human GABAA receptor alpha 1, subunit is essential for GABA binding and chloride ion current gating. Westh-Hansen SE, Witt MR, Dekermendjian K, Liljefors T, Rasmussen PB, Nielsen M. Neuroreport. (1999) 10(11):2417-21.

[h] The GABAA receptor alpha 1 subunit Pro174-Asp191 segment is involved in GABA binding and channel gating. Newell JG, Czajkowski C. J Biol Chem. (2003) 278(15):13166-72.

[j] Mapping the rho1 GABA(C) receptor agonist binding pocket. Constructing a complete model. Sedelnikova A, Smith CD, Zakharkin SO, Davis D, Weiss DS, Chang Y. J Biol Chem. (2005) 280(2):1535-42.

[k] Homomeric rho 1 GABA channels: activation properties and domains. Amin J, Weiss DS. Receptors Channels. (1994) 2(3):227-36.

[l] A cation-pi binding interaction with a tyrosine in the binding site of the GABAC receptor. Lummis SC, L Beene D, Harrison NJ, Lester HA, Dougherty DA. Chem Biol. (2005) 12(9):993-7.

[m] Locating the carboxylate group of GABA in the homomeric rho GABA(A) receptor ligand-binding pocket. Harrison NJ, Lummis SC. J Biol Chem. (2006) 281(34):24455-61.

Table S2 – Overview of mutagenesis of residues involved in benzodiazepine binding and/or allosteric modulation in $GABA_A$ receptors and sequence conservation in ELIC

		$GABA_AR$	ELIC
loop A	α1 (+)	D97 [a] F99 [a] H101 [abcde] G157 [a]	A75 E77 I79 E131
loop B	α1 (+)	Y159 [f] A160 [a] Y161 [q]	F133 S134 Y135
loop C	α1 (+)	G200 [ag] S204 [r] S205 [h] T206 [aij] Y209 [afj]	S171 Y175 D176 S179 F188
loop D	γ2 (-)	D75 [k] I76 [k] F77 [klm] A79 [kno] T81 [ko]	D36 G37 Y38 V40 Q42
loop E	γ2 (-)	R144 [a] M130 [ap] R132 [a]	R105 R91 M93
loop F	γ2 (-)	R197 [a]	E156
loop G	γ2 (-)	Y58 [n]	F19

[a] Different residues in the GABAA receptor benzodiazepine binding pocket mediate benzodiazepine efficacy and binding. Morlock EV, Czajkowski C. Mol Pharmacol. 2011 80 (1):14-22

[b] A single histidine in GABAA receptors is essential for benzodiazepine agonist binding. Wieland HA, Lüddens H, Seeburg PH. J Biol Chem. (1992) 267(3):1426-9.

[c] Four amino acid exchanges convert a diazepam-insensitive, inverse agonist preferring GABAA receptor into a diazepam-preferring GABAA receptor. Wieland HA, Lüddens H. J Med Chem. (1994) 37(26):4576-80.

[d] Mutagenesis of the rat alpha1 subunit of the gamma-aminobutyric acid(A) receptor reveals the importance of residue 101 in determining the allosteric effects of benzodiazepine site ligands. Dunn SM, Davies M, Muntoni AL, Lambert JJ. Mol Pharmacol. (1999) 56(4):768-74.

[e] Structural requirements for ligand interactions at the benzodiazepine recognition site of the GABA(A) receptor. Davies M, Bateson AN, Dunn SM. J Neurochem. (1998) 70(5):2188-94.

[f] Two tyrosine residues on the alpha subunit are crucial for benzodiazepine binding and allosteric modulation of gamma-aminobutyric acidA receptors. Amin J, Brooks-Kayal A, Weiss DS. Mol Pharmacol. (1997) 51(5):833-41.

[g] Amino acid residue 200 on the alpha1 subunit of GABA(A) receptors affects the interaction with selected benzodiazepine binding site ligands. Schaerer MT, Buhr A, Baur R, Sigel E. Eur J Pharmacol. (1998) 354(2-3):283-7.

[h] Identification of a residue in the gamma-aminobutyric acid type A receptor alpha subunit that differentially affects diazepam-sensitive and -insensitive benzodiazepine site binding.
Derry JM, Dunn SM, Davies M. J Neurochem. (2004) 88(6):1431-8.

[i] Amino acid residue 200 on the alpha1 subunit of GABA(A) receptors affects the interaction with selected benzodiazepine binding site ligands. Schaerer MT, Buhr A, Baur R, Sigel E. Eur J Pharmacol. (1998) 354(2-3):283-7.

[j] Residues at positions 206 and 209 of the alpha1 subunit of gamma-aminobutyric AcidA receptors influence affinities for benzodiazepine binding site ligands. Buhr A, Schaerer MT, Baur R, Sigel E. Mol Pharmacol. (1997) 52(4):676-82.
[k] A (beta)-strand in the (gamma)2 subunit lines the benzodiazepine binding site of the GABA A receptor: structural rearrangements detected during channel gating. Teissére JA, Czajkowski C. J Neurosci. (2001) 21(14):4977-86.
[l] Key amino acids in the gamma subunit of the gamma-aminobutyric acidA receptor that determine ligand binding and modulation at the benzodiazepine site. Wingrove PB, Thompson SA, Wafford KA, Whiting PJ. Mol Pharmacol. (1997) 52(5):874-81.
[m] Subtle changes in residue 77 of the gamma subunit of alpha1beta2gamma2 GABAA receptors drastically alter the affinity for ligands of the benzodiazepine binding site. Buhr A, Baur R, Sigel E. J Biol Chem. (1997) 272(18):11799-804.
[n] Identification of benzodiazepine binding site residues in the gamma2 subunit of the gamma-aminobutyric acid(A) receptor. Kucken AM, Wagner DA, Ward PR, Teissére JA, Boileau AJ, Czajkowski C. Mol Pharmacol. (2000) 57(5):932-9.
[o] Structural requirements for imidazobenzodiazepine binding to GABA(A) receptors. Kucken AM, Teissére JA, Seffinga-Clark J, Wagner DA, Czajkowski C. Mol Pharmacol. (2003) 63(2):289-96.
[p] A point mutation in the gamma2 subunit of gamma-aminobutyric acid type A receptors results in altered benzodiazepine binding site specificity. Buhr A, Sigel E. Proc Natl Acad Sci U S A. (1997) 94(16):8824-9.
[q] Point mutations of the alpha 1 beta 2 gamma 2 gamma-aminobutyric acid(A) receptor affecting modulation of the channel by ligands of the benzodiazepine binding site. Buhr A, Baur R, Malherbe P, Sigel E. Mol Pharmacol. (1996) 49(6):1080-4.
[r] Structural elements of the gamma-aminobutyric acid type A receptor conferring subtype selectivity for benzodiazepine site ligands. Renard S, Olivier A, Granger P, Avenet P, Graham D, Sevrin M, George P, Besnard F. J Biol Chem. (1999) 274(19):13370-4.

Table S3 – Crystallographic and refinement statistics

	GABA + flurazepam	Br-flurazepam	zopiclone
Crystallographic statistics			
Beamline	PROXIMA-I (SOLEIL)	PROXIMA-I (SOLEIL)	X06A (SLS)
Date of collection	21-May-2010	30-Mar-2011	2-Jun-2011
Wavelength (Å)	0.98011	0.91936	0.9999
Spacegroup	$P2_1$	$P2_1$	$P2_1$
a,b,c (Å)	105.77, 266.51, 110.98	106.11, 268.10, 111.54	105.40, 266.83, 110.76
β (°)	108.82	108.10	109.02
Resolution limits (Å)	24.98 - 3.80 (4.01 - 3.80)	44.63 - 3.61 (3.80 - 3.61)	43.95 - 3.34 (3.52 - 3.34)
R_{merge} (%)	12.4 (74.1)	18.5 (76.6)	10.8 (66.9)
$\langle I/\sigma \rangle$	8.0 (2.1)	11.3 (1.9)	12.8 (2.2)
Multiplicity	3.8 (3.6)	11.4 (3.6)	3.8 (3.8)
Completeness (%)	95.7 (96.3)	99.6 (97.7)	99.6 (98.5)
Total number of reflections	205050 (28620)	767256 (34452)	318468 (45278)
Number unique reflections	54291 (7938)	67378 (9626)	83009 (11960)
Anomalous completeness		98.9 (93.3)	
Anomalous multiplicity		5.7 (1.8)	
Refinement and model statistics			
R_{work} (%)	18.52	23.06	21.11
R_{free} (%)	22.99	24.54	26.65
Rmsd bond distance (Å)	0.005	0.008	0.013
Rmsd bond angle (°)	1.099	0.910	1.686
Average B-factors			
Protein	131.53	137.73	120.19
GABA	139.28		
Flurazepam	183.95		
Br-flurazepam		164.51	
Zopiclone			89.45

Figure S1 – Sequence alignment of ELIC and other pLGICs

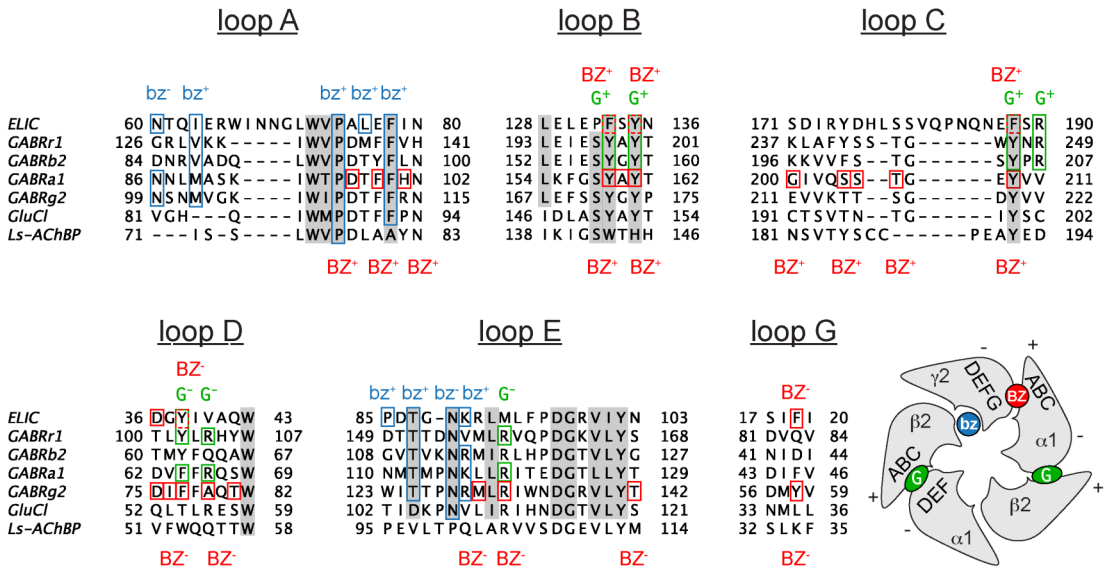

Sequence alignment of the loop regions of ELIC and related subunits showing residues important for GABA (G) binding (in green). Residues contributing to the high affinity benzodiazepine binding site (BZ) in $GABA_A$ receptors are shown in red and the intrasubunit benzodiazepine site (bz) in ELIC are shown in blue. The cartoon in the lower right corner illustrates the subunit arrangement of a typical $GABA_A$ receptor showing the location of GABA and benzodiazepine binding sites.

Figure S2 – Activation of ELIC by GABA

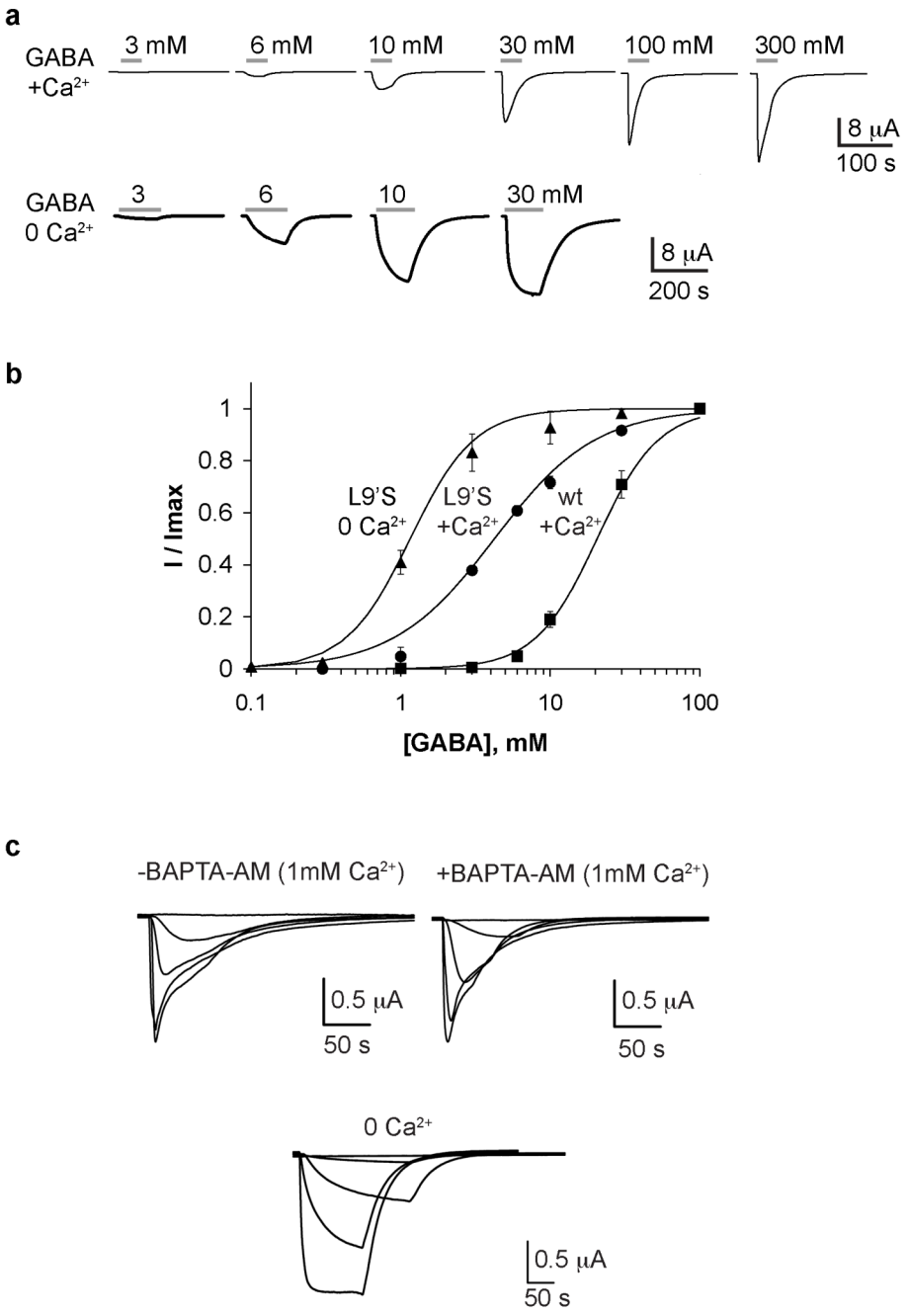

a Example traces of ELIC responses obtained upon application of increasing concentrations of GABA in the presence (+Ca^{2+}) and absence (0 Ca^{2+}) of calcium ions in the extracellular recording solution. **b** Concentration-response relationships from wt ELIC, L240S ELIC containing a mutation at the 9' position of the pore-lining M2-helix in the presence and absence of Ca^{2+}. EC_{50}-values are 21 mM at wt ELIC in +Ca^{2+} (Hill slope = 2.1), 7.3 mM at wt ELIC in 0 Ca^{2+} (Hill slope = 3.5), 4.2 mM at L9'S in +Ca^{2+} (Hill slope = 1.3) and 1.2 mM at L9'S in 0 Ca^{2+} (Hill slope = 2.0). All concentrations were tested in 4-6 oocytes. **c** Incorporation of BAPTA into oocytes, or experiments performed in the presence of niflumic or fluflenamic acid (data not shown) does not change the effects of Ca^{2+}, showing that these effects are not caused by endogenous Ca^{2+}-activated Cl^- channels in oocytes.

Figure S3 – Structure formulas of bromo-analogs of benzodiazepines

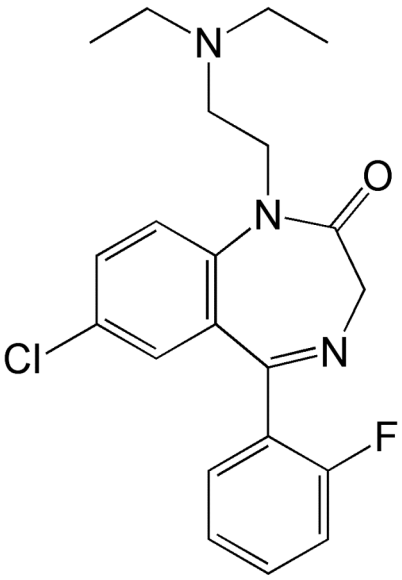

flurazepam

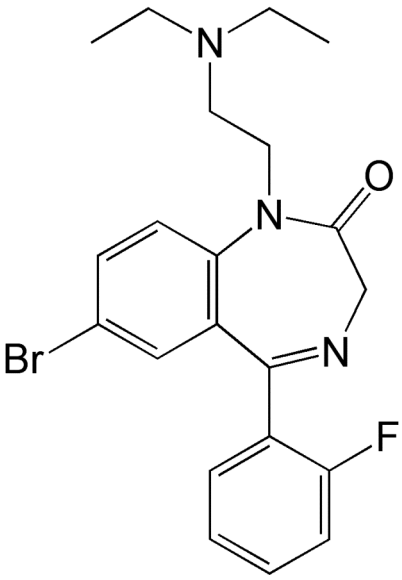

bromo-flurazepam

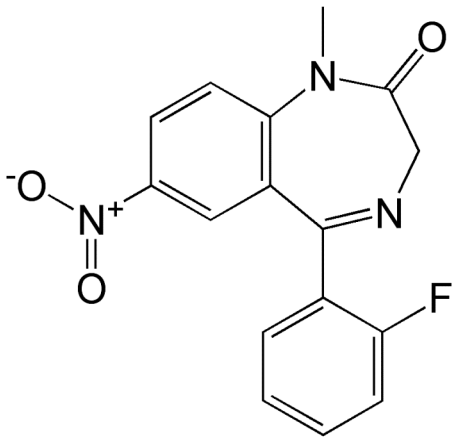

flunitrazepam

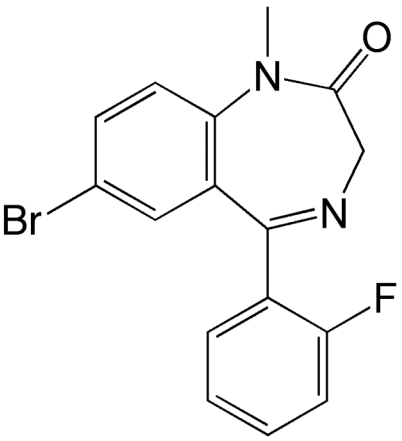

bromo-flunitrazepam

Figure S4 – F_o-F_c Fourier density for ELIC in complex with GABA

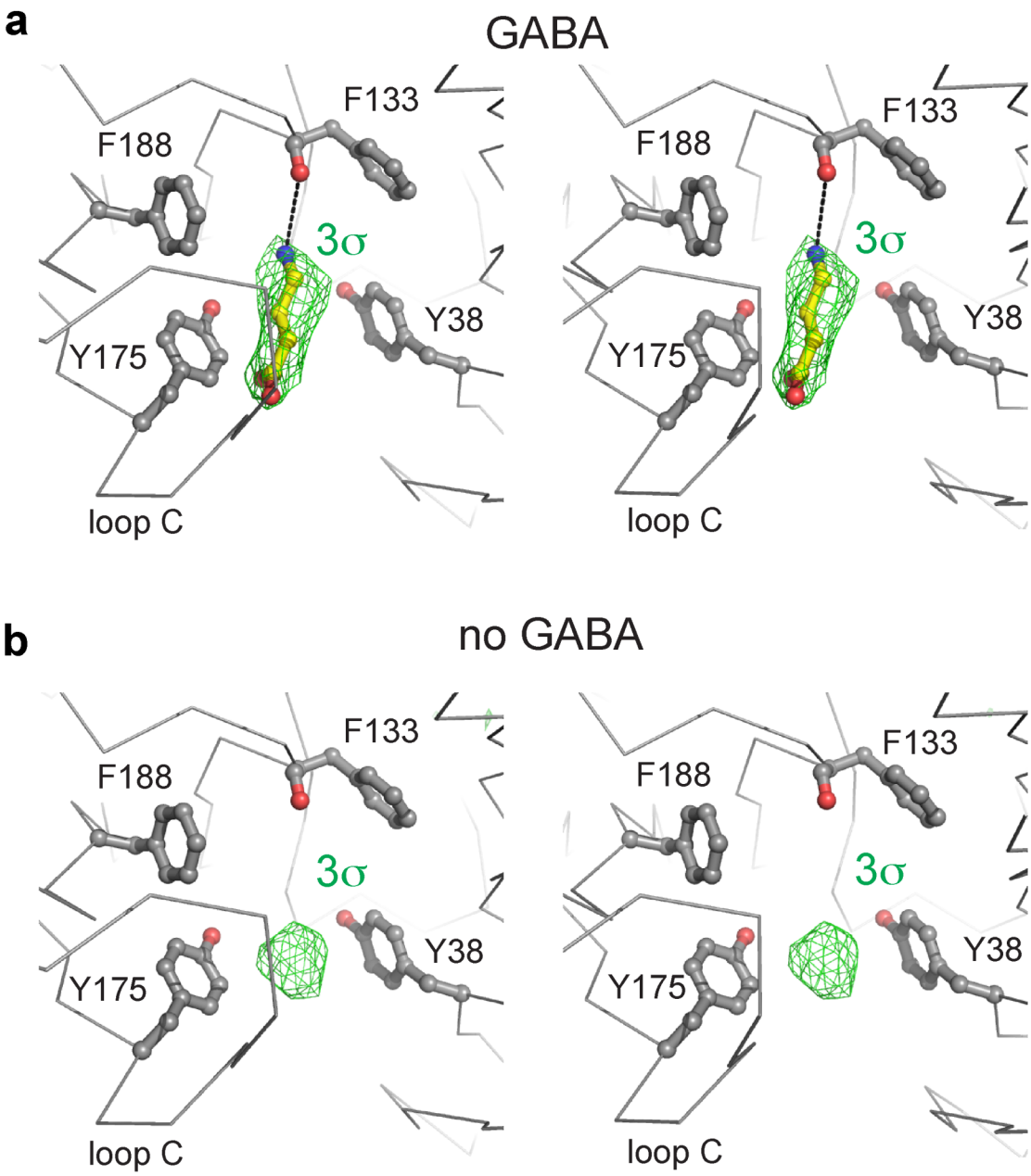

a Stereo representation of sausage-shaped Fourier difference density (green, 3σ) observed in the ligand binding site of ELIC. Crystals were grown in the presence of GABA and flurazepam (FZM). GABA is shown in yellow ball and stick representation. Important aromatic residues of the ligand binding site are show in grey ball and stick representation. The dashed line represents a hydrogen bond between the carbonyl oxygen of F133 and the γ-amino nitrogen of GABA.

Such density could not be observed from ELIC crystals grown in the absence of GABA, as shown in panel **b**. Spherical density was also observed in the published ELIC structure from Hilf and Dutzler (Nature, 2008) and this was interpreted by the authors as a possible water molecule or ion bound in the ligand binding site. The electron density shown in panel b is calculated from our diffraction data at the same resolution as data shown in panel a.

Figure S5 – Unnatural amino acid mutagenesis of the GABA binding pocket

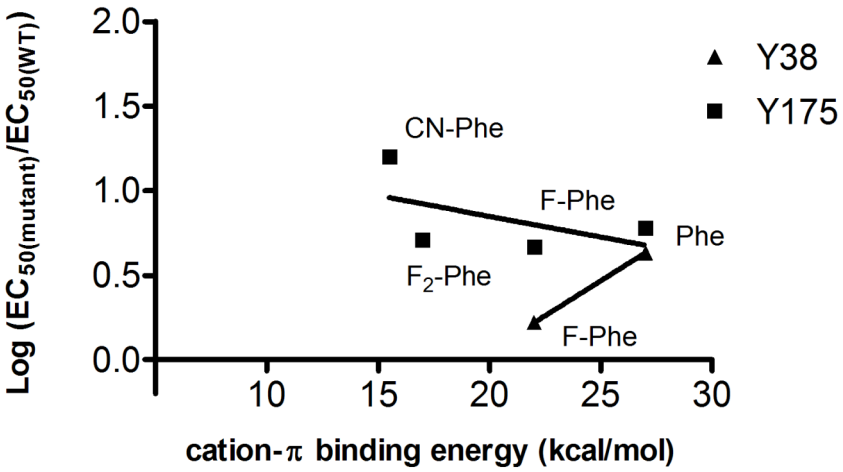

Unnatural amino acid mutagenesis for residues Y38 and Y175 in the GABA binding pocket does not reveal a clear correlation between EC_{50}-value and the cation-π binding ability of phenylalanine derivatives, suggesting that these residues are not involved in a cation-π interaction with the γ-amino group of GABA.

Figure S6 – Stereo representation of ligand electron density maps for flurazepam

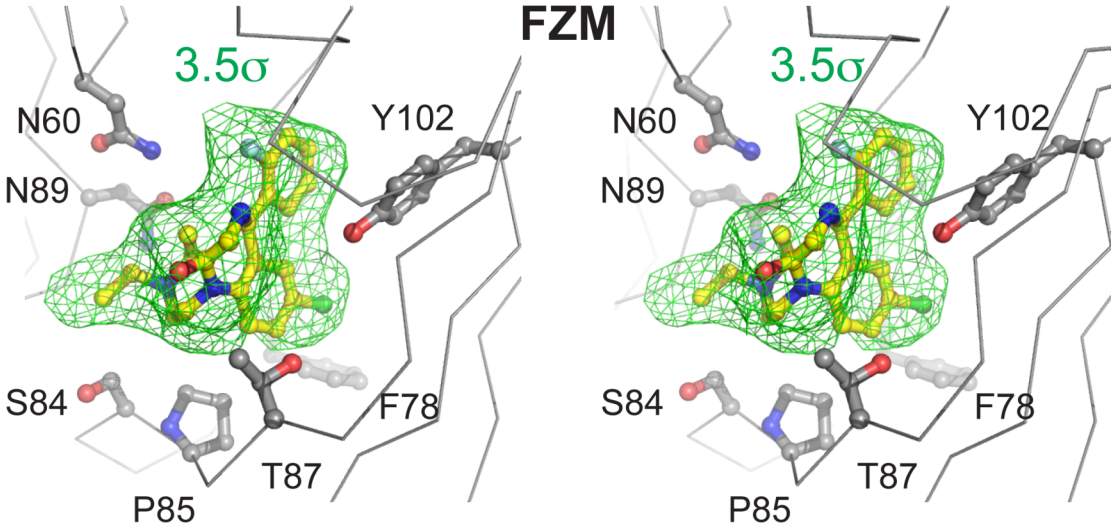

The green mesh represents F_o-F_c difference density for flurazepam (FZM) at the intrasubunit benzodiazepine site. Flurazepam is shown in yellow ball and stick representation. Surrounding residues are shown in grey. Oxygen=red, nitrogen=blue, chlorine=green and fluorine=white.

Figure S7 – Mutagenesis of the intrasubunit and intersubunit benzodiazepine site

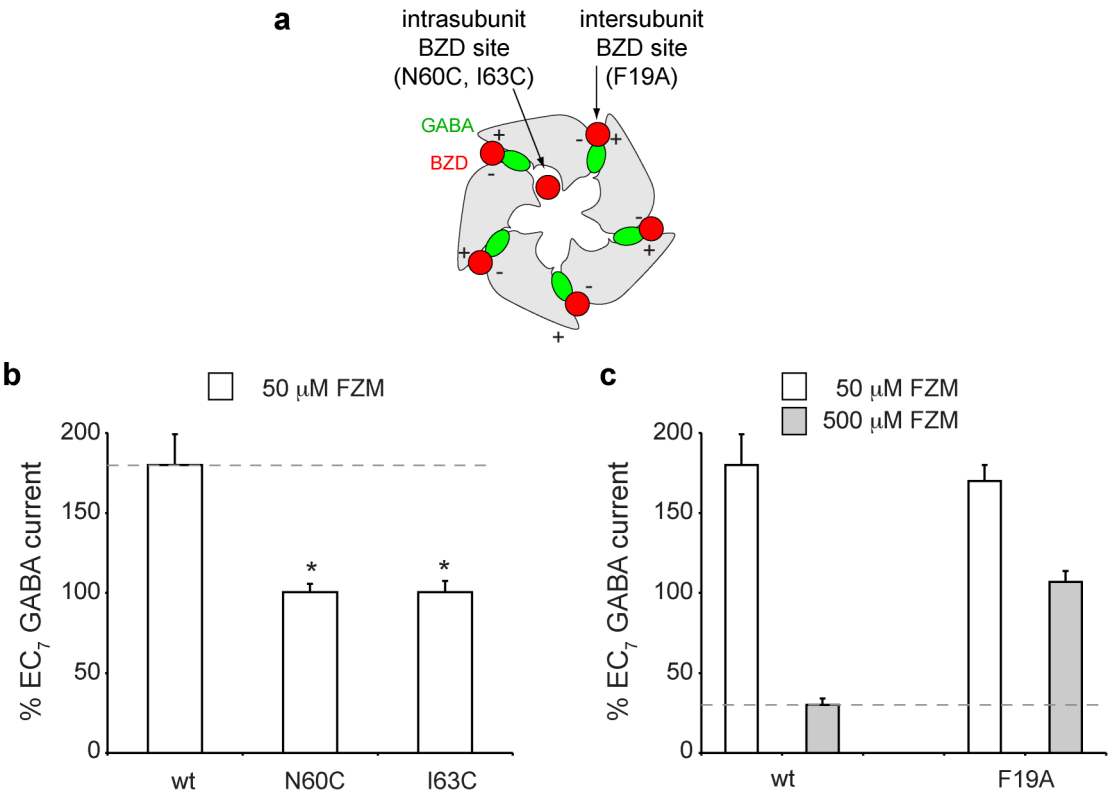

a Cartoon representation of intrasubunit and intersubunit benzodiazepine sites in ELIC. **b** Potentiation of GABA responses by 50 μM flurazepam (FZM) is eliminated in N60C and I63C, two positions that line the intrasubunit benzodiazepine site. **c** The inhibitory effect of 500 μM FZM is eliminated in F19A, a residues that lines the intersubunit benzodiazepine site. The F19A mutation has no effect on the potentiation by 50 μM FZM. Together, these data indicate that the intrasubunit site mediates potentiation and that the intersubunit site mediates inhibition by FZM. (data = mean ± sem, n=3-8). * indicates significant difference ($P<0.05$).

Figure S8 – Anomalous difference density maps and F_o-F_c Fourier density for ELIC in complex with Br-flurazepam

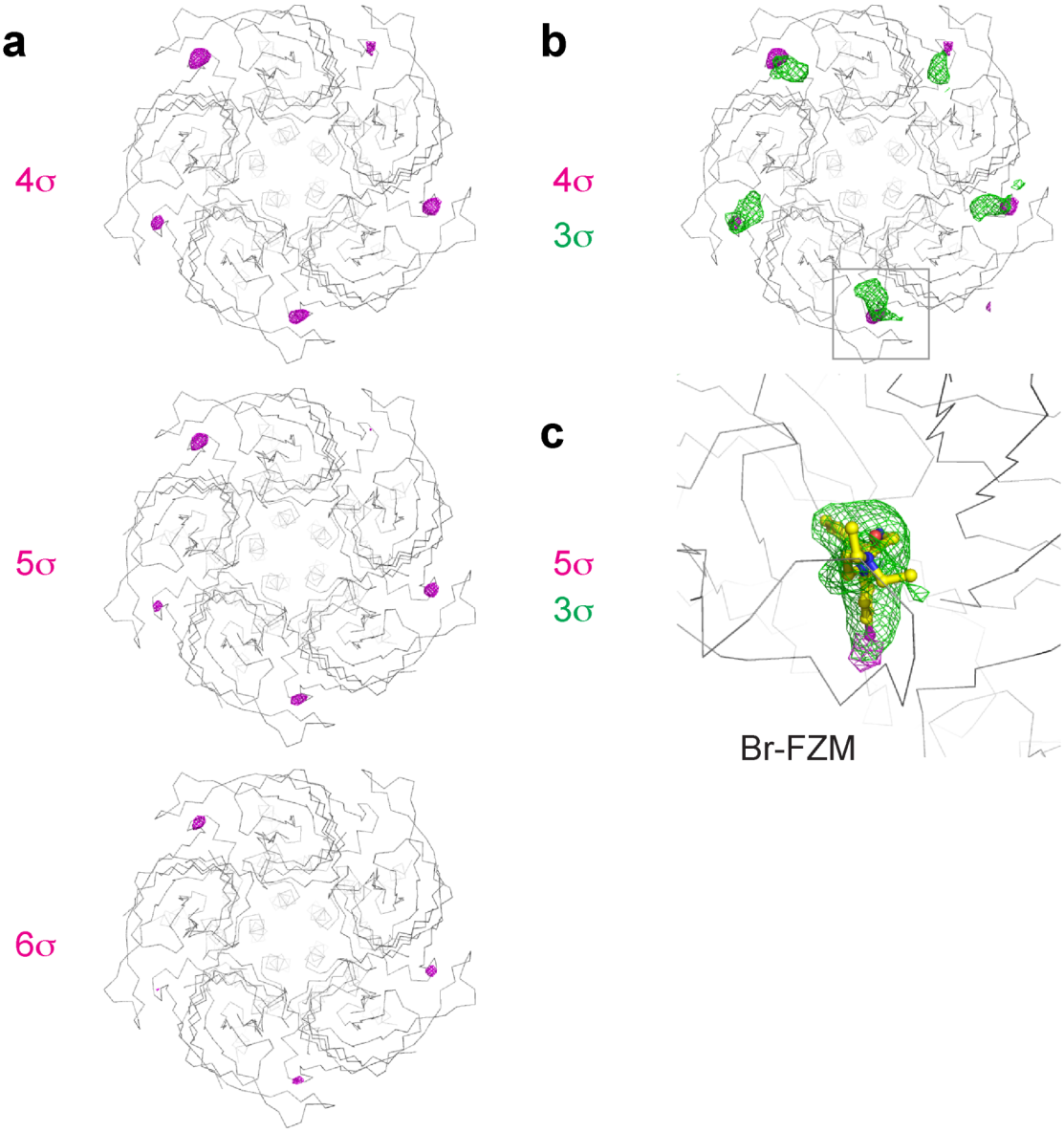

a Anomalous difference density contoured at 4, 5 and 6σ (magenta mesh) shows the location of the bromine atom in all five binding sites of the ELIC pentamer. **b** Overlay of anomalous different density (4σ, magenta) and F_o-F_c difference density (3σ, green). **c** Detailed view of electron density at one binding site in which Br-flurazepam (Br-FZM) was built (yellow ball and stick representation).

Figure S9 – Stereo representation of ligand electron density maps for Br-flurazepam and zopiclone

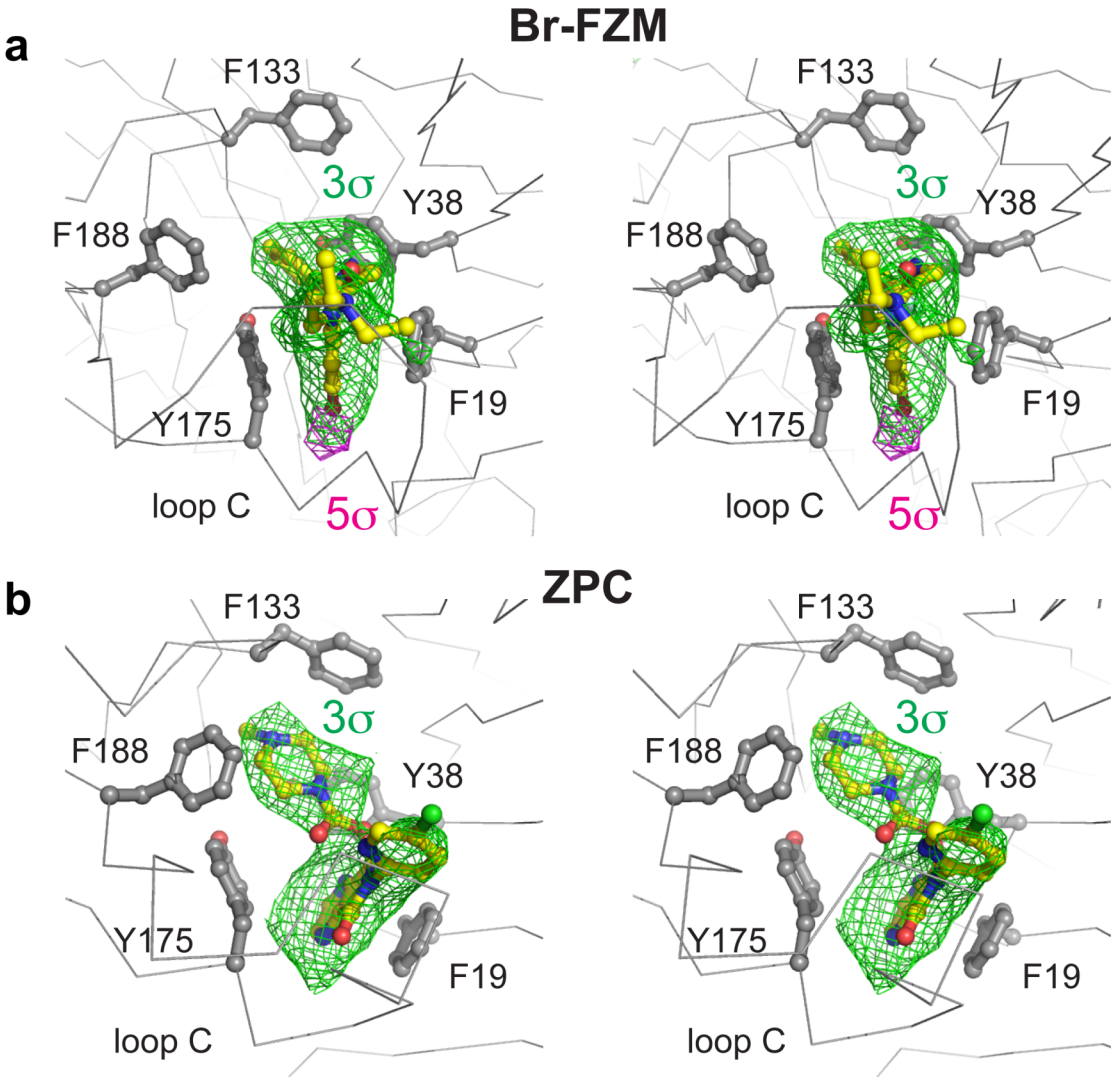

The green mesh represents F_o-F_c difference density Br-flurazepam (Br-FZM, panel **a**) and zopiclone (ZPC, panel **b**) at the intersubunit benzodiazepine site. The purple mesh in panel **b** represents anomalous density for the Bromine atom. Ligands are shown in yellow ball and stick representation. Surrounding residues are shown in grey. Oxygen=red, nitrogen=blue, chlorine=green and bromine=magenta.

Figure S10 – Conformational change of loop C in different ELIC structures

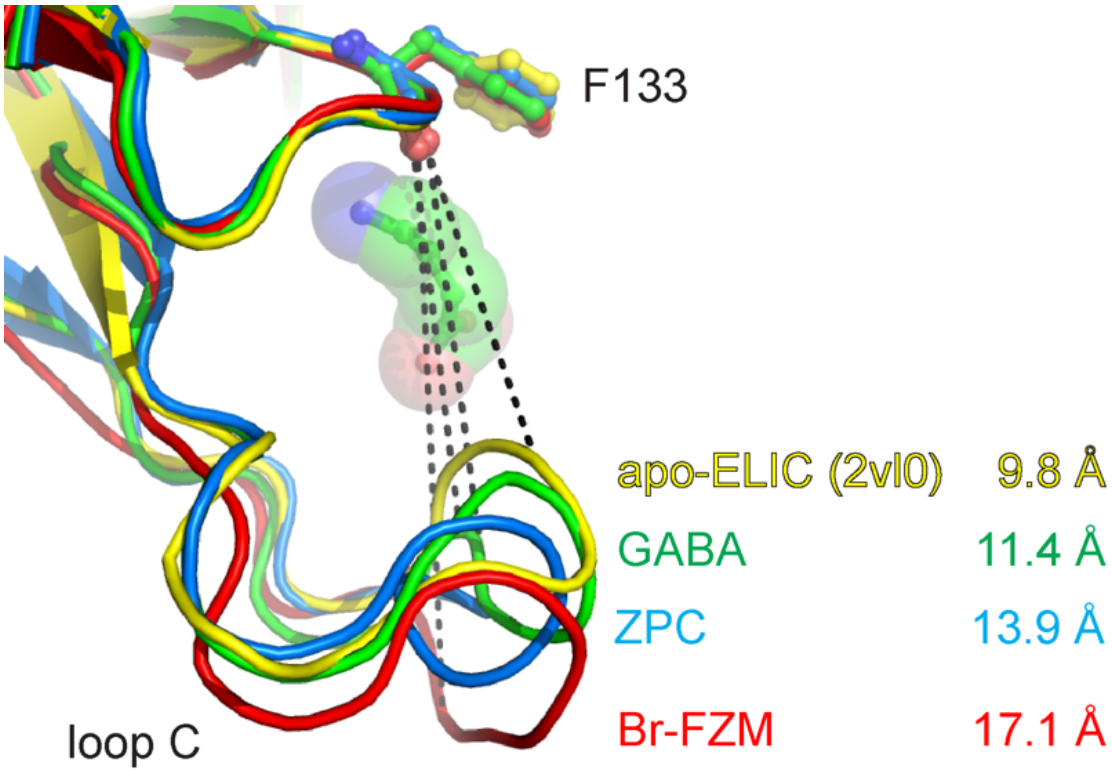

Loop C undergoes conformational changes upon GABA and benzodiazepine binding. We quantified the extension of loop C by measuring the distance between the carbonyl oxygen of F133 (loop B) and the Cα atom of L178 at the tip of loop C. The numeric values are the average of distances measured in 10 different subunits of 2 pentamers in the asymmetric unit. GABA is shown in stick representation with transparent spheres.

Figure S11 – Stereo representation of electron density maps near loop C

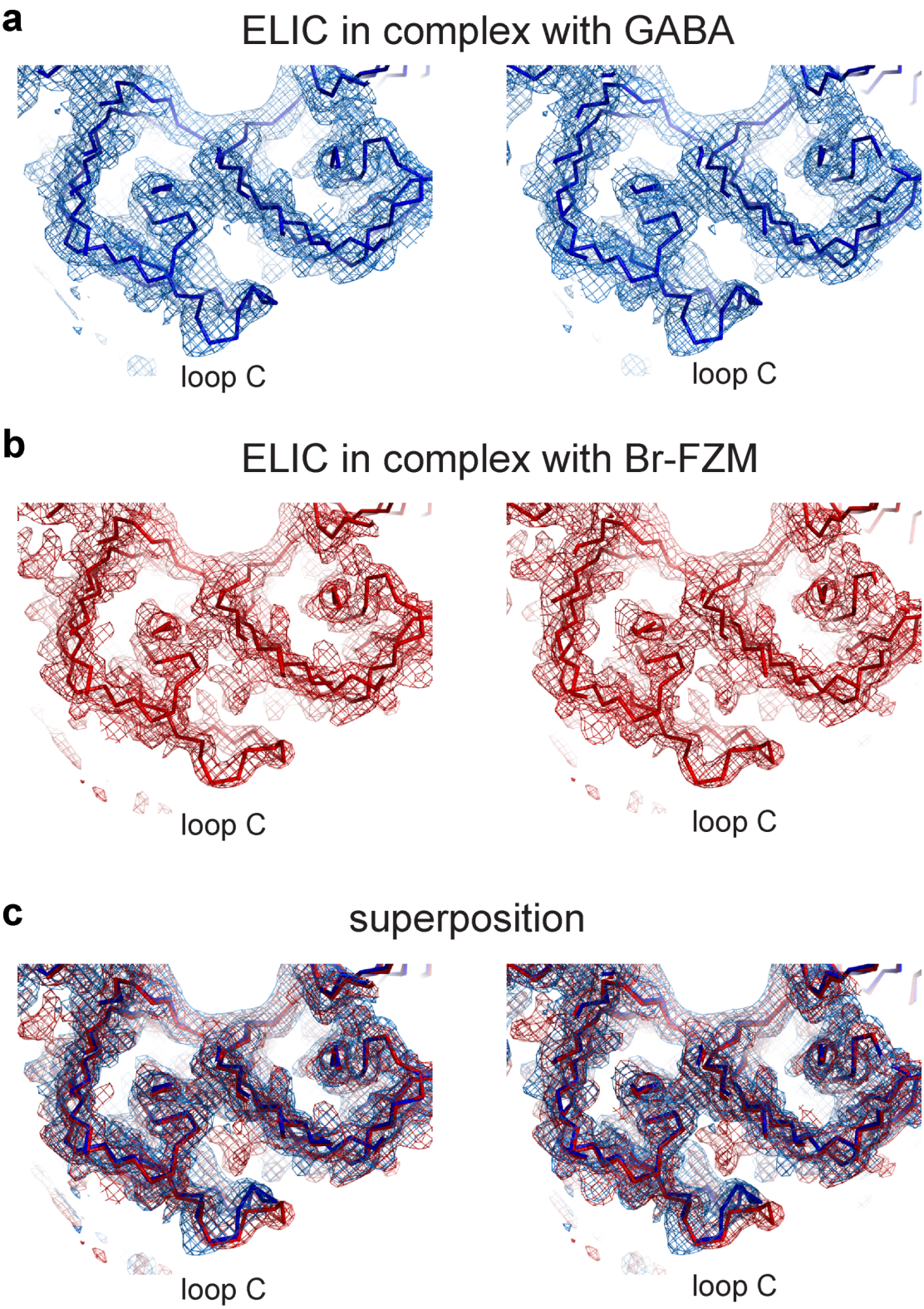

5-fold averaged electron density maps contoured at 1.5σ were used to build loop C in the ELIC complex with GABA (**a**) and Br-Flurazepam (Br-FZM, **b**). Panel **c** shows an overlay of the map for GABA (blue) and Br-FZM (red).

Figure S12 – Chemical synthesis of Br-flurazepam and Br-flunitrazepam

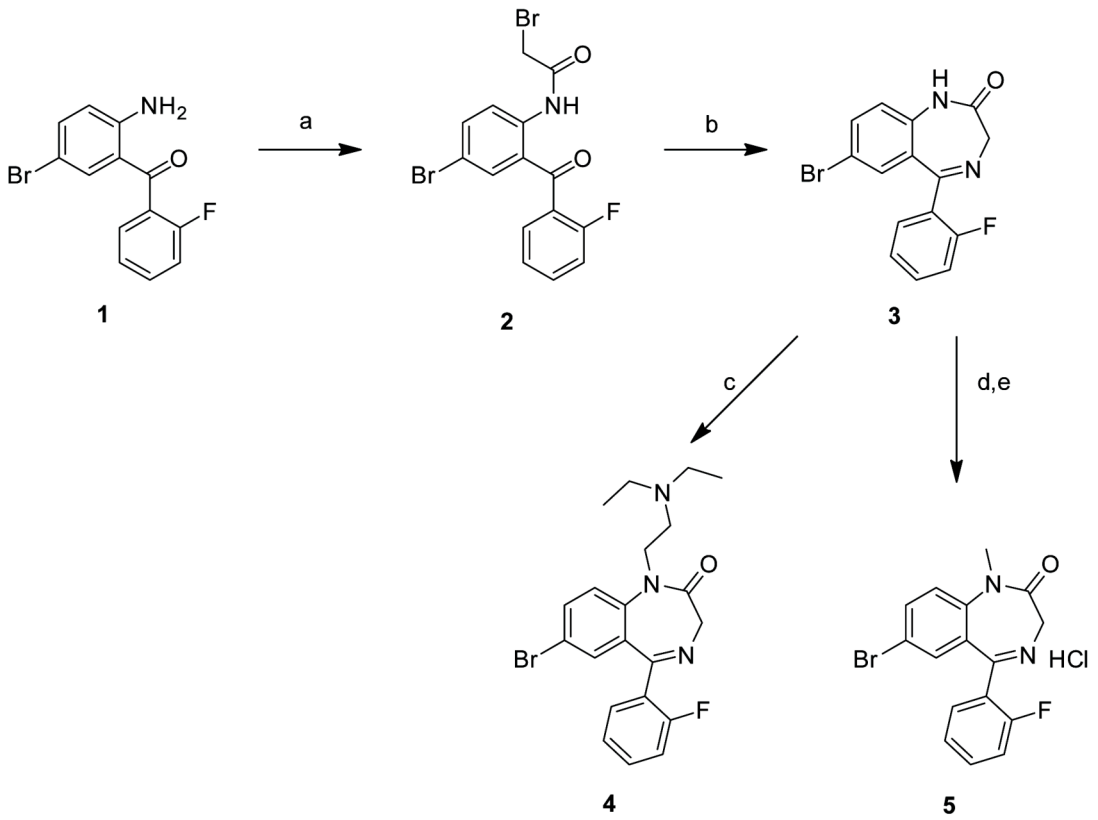

a: 2-bromoacetyl bromide, MeCN, room temperature, 2h; **b**: 7N ammonia in MeOH, room temperature, 20h; **c**: 2-chloro-*N*,*N*-diethylethanamine, Aliquat 336, toluene, 50% NaOH(aq), rt, 18h; **d**: Methyliodide, Aliquat 336, toluene, 50% NaOH(aq), rt, 18h; **e**: 2M HCl dioxane/ether

The synthesis of benzodiazepine **5** and the novel compound Br-flurazepam **4** was synthesized according to the following protocol. First, compound **1** was reacted with bromoacetobromide in acetonitrile for 2 hours at room temperature to yield **2**. Upon stirring of this intermediate in ammonia in methanol (7N) for 20 hours compound **3** was formed. Finally, applying phase transfer catalyst chemistry both compounds **4** and **5** were successfully synthesized and characterized as described in detail below.

Chemicals and solvents were purchased from Aldrich and used as received. Unless indicated otherwise, all reactions were carried out under an inert atmosphere of dry N_2. TLC analyses were performed with Merck F254 alumina silica plates using UV visualization or staining. Column purifications were carried out automatically using the Biotage equipment. All HRMS spectra were recorded on Bruker microTOF mass spectrometer using ESI in positive ion mode. ^{1}H NMR spectra were recorded on a Bruker 250 (250 MHz) or a Bruker 500 (500 MHz) spectrometer. Data are reported as follows: chemical shift, integration, multiplicity (s = singlet, d = doublet, t = triplet, br = broad, m = multiplet), and coupling constants (Hz). Chemical shifts are reported in ppm with the natural abundance of deuterium in the solvent as the internal reference ($CHCl_3$ in $CDCl_3$: δ 7.26 and CH_3OH in CH_3OD: δ 3.31). ^{13}C NMR spectra were recorded on a Bruker 500 (126 MHz) spectrometer with complete proton

decoupling. Chemical shifts are reported in ppm with the solvent resonance resulting from incomplete deuteration as the internal reference ($CDCl_3$: δ 77.16, CH_3OD: δ 49.00). In the case of coupling to fluor, the data are reported as follows: chemical shift, multiplicity (d = doublet), coupling constants (C-F, Hz). Melting points were taken using the Stanford Research Systems Optimelt apparatus, and values given are uncorrected. Systematic names for molecules according to IUPAC rules were generated using the Chemdraw AutoNom program. Unless specified otherwise, all compounds have a purity of ≥95%. This was determined using a Shimadzu HPLC/MS workstation with a LC-20AD pump system, SPD-M20A diode array detection, and a LCMS-2010 EV liquid chromatograph mass spectrometer. The column used is an Xbridge C18 5 μm column (100 mm × 4.6 mm). Compound purities were calculated as the percentage peak area of the analyzed compound by UV detection at 230 nm. Solvents used were the following: solvent B = MeCN 0.1% Formic Acid; solvent A = water 0.1%. The analysis was conducted using a flow rate of 1.0 mL/min, start 5% B, linear gradient to 90% B in 4.5 min, then 1.5 min at 90% B, linear gradient to 5% B in 0.5 min and then 1.5 min at 5% B, total run time of 8 min.

2-bromo-N-(4-bromo-2-(2-fluorobenzoyl)phenyl)acetamide (**2**). A mixture of (2-amino-5-bromophenyl)(2-fluorophenyl)methanone (**1**) (3.10 g, 10.5 mmol) and potassiumcarbonate (7.28g, 52.7 mmol) in acetonitrile (30 ml) was stirred at 0ºC. After 5 min a solution of 2-bromoacetyl bromide (4.25g, 21.1 mmol) in acetonitrile (5 ml) was added dropwise. The resulting suspension was stirred at room temperature for 2 hours after which the solvent was removed under reduced presure. Water (100 ml) and dichloromethane (100 ml) were added, the organic layer was separated and the aqueous layer was extracted with dichloromethane (2 x 50 ml). The organic layers were combined, dried (Na_2SO_4) and concentrated *in vacuo* to yield 2 as a light yellow solid (4.32 g, 10.4 mmol, 99% yield). ^{1}H NMR (250 MHz, $CDCl_3$) δ (ppm) 11.79 (s, 1H), 8.63 (d, *J* = 8.98 Hz, 1H), 7.71 (dd, *J* = 8.97, 2.35 Hz, 1H), 7.63 – 7.44 (m, 3H), 7.38 – 7.13 (m, 2H), 4.04 (s, 2H). m.p. 131-132 ºC, LCMS: ret. time 5.26 min, purity 100%.

7-bromo-5-(2-fluorophenyl)-1H-benzo[e][1,4]diazepin-2(3H)-one (3). To a round bottom flask were added 2-bromo-N-(4-bromo-2-(2-fluorobenzoyl)phenyl)acetamide (2) (0.83 g, 2 mmol) and 7N ammonia in methanol (20 ml), the resulting suspension was stirred at room temperature for 20h. The solvent was evaporated and the residue purified by flash chromatography (silica gel; dichloromethane: triethylamine = 99:1) to yield 3 as a beige solid (0.59 g, 1.75 mmol, 88% yield). ^{1}H NMR (250 MHz, CDCl3) δ (ppm) 9.39 (s, 1H), 7.62 – 7.41 (m, 3H), 7.36 – 7.01 (m, 4H), 4.38 (s, 2H). m.p. 120-121 ºC, LCMS: ret. time 4.14 min, purity 97%, $M+H]^+$ 332.80

7-bromo-1-(2-(diethylamino)ethyl)-5-(2-fluorophenyl)-1H-benzo[e][1,4]diazepin-2(3H)-one (4). To a solution of 7-bromo-5-(2-fluorophenyl)-1H-benzo[e][1,4]diazepin-2(3H)-one (3) (333 mg, 1mmol) in toluene (15 ml) were added 50% NaOH (aq) (15 ml), 2-chloro-N,N-diethylethanaminium chloride (172 mg, 1 mmol) and N-methyl-N,N-dioctyloctan-1-aminium chloride (20 mg, 0.05 mmol). The resulting mixture was stirred vigorously at room temperature for 18 hours. The organic layer was separated and the aqueous layer was extracted with toluene (2x 30 ml), the organic layers were combined, washed with water (2 x 30 ml), dried

(Na_2SO_4) and concentrated *in vacuo*. The residue was purified by flash chromatography (silica gel; gradient ethylacetate: heptane = 5:95 to 80:20) to yield 4 as an oil (92 mg, 0.22 mmol, 22% yield). ^{1}H NMR (500 MHz, $CDCl_3$) δ (ppm) 7.69 – 7.59 (m, 2H), 7.50 (d, *J* = 8.93 Hz, 1H), 7.49 – 7.44 (m, 1H), 7.29 (d, *J* = 2.11 Hz, 1H), 7.28 – 7.23 (m, 1H), 7.12 – 7.03 (m, 1H), 4.85 (d, *J* = 10.46 Hz, 1H), 4.36 – 4.24 (m, 1H), 3.80 – 3.67 (m, 2H), 2.67 – 2.46 (m, 6H), 0.95 (t, 6H). ^{13}C NMR (126 MHz, $CDCl_3$) δ 168.18, 165.78, 160.54 (d, $^1J_{CF}$ = 252 Hz), 140.98, 134.32, 132.60, 132.36 (d, $^3J_{CF}$ = 9 Hz), 131.28 (d, $^3J_{CF}$ = 3 Hz), 131.16 (d, $^5J_{CF}$ = 1 Hz), 126.71 (d, $^2J_{CF}$ = 11 Hz), 124.51, 124.47 (d, $^4J_{CF}$ = 4 Hz), 117.52, 116.26 (d, $^2J_{CF}$ = 23 Hz), 57.07, 50.44, 47.38, 47.38, 46.43, 11.80, 11.80. LCMS: ret. time 3.59 min, purity 98%, $M+H]^+$ 431.90, HRMS *m/z*: $[M+H]^+$ calcd for $C_{21}H_{23}BrFN_3O$: 432.1081, found: 432.1031.

7-bromo-5-(2-fluorophenyl)-1-methyl-2-oxo-2,3-dihydro-1H-benzo[e][1,4]diazepin-4-ium chloride (5). To a solution of 7-bromo-5-(2-fluorophenyl)-1H-benzo[e][1,4]diazepin-2(3H)-one (**3**) (230 mg, 0.69mmol) in toluene (15 ml) were added 50% NaOH (aq) (15 ml), iodomethane (196 mg, 1.38 mmol) and N-methyl-N,N-dioctyloctan-1-aminium chloride (14 mg, 0.05 mmol). The resulting mixture was stirred vigorously at room temperature for 18 hours. The organic layer was separated and the aqueous layer was extracted with toluene (2x 30 ml), the organic layers were combined, washed with water (2 x 30 ml), dried (Na_2SO_4) and concentrated *in vacuo*. The residue was purified by flash chromatography (silica gel; gradient ethylacetate: heptane = 5:95 to 80:20). The obtained product was dissolved in diethylether (5 ml) and transformed to the corresponding HCl salt by addition of 2M HCl in dioxane (10ml) while stirring. The precipitate was collected by filtration and dried *in vacuo* to yield **5** as a white solid (147 mg, 0.38 mmol, 55% yield). ^{1}H NMR (500 MHz, MeOD) δ (ppm) 8.09 (dd, *J* = 8.97, 2.38 Hz, 1H), 7.94 – 7.86 (m, 1H), 7.72 – 7.66 (m, 2H), 7.57 (d, *J* = 2.33 Hz, 1H), 7.54 – 7.49 (m, 1H), 7.48 – 7.42 (m, 1H), 4.67 (d, *J* = 13.11 Hz, 1H), 4.33 (d, *J* = 13.20 Hz, 1H), 3.52 (s, 3H). ^{13}C NMR (126 MHz, MeOD) δ 173.55, 168.13, 162.27 (d, $^1J_{CF}$ = 257 Hz), 145.74, 140.83, 139.01 (d, $^3J_{CF}$ = 9 Hz), 136.01, 134.74 (d, $^3J_{CF}$ = 1 Hz), 127.27, 126.78 (d, $^4J_{CF}$ = 4 Hz), 126.23, 121.28, 119.37, 118.35 (d, $^2J_{CF}$ = 21 Hz), 52.73, 36.33. m.p. 174-175 ºC, LCMS: ret. time 4.47 min, purity 100%, $M+H]^+$ 346.80, HRMS *m/z*: $[M+H]^+$ calcd for $C_{16}H_{12}BrFN_2O$: 347.0190, found: 347.0155.